#### RESEARCH



# Calibration and Release of Magnetograms/Dopplergrams Obtained at the Mt. Wilson 150-Foot Tower Telescope (MWO)

Roger K. Ulrich<sup>1</sup> • John Boyden<sup>1</sup> • Tham Tran<sup>1</sup>

Received: 22 June 2024 / Accepted: 9 October 2024 / Published online: 25 October 2024 © The Author(s) 2024

#### Abstract

The Mt. Wilson Observatory archive of observations of solar disk magnetic fields, Doppler velocities, and spectral line intensities is a resource for studying the Sun's state from 1967 to 2013. Instrument changes/upgrades during this time must be considered when interpreting this record. Portions of this record have been previously released. This publication documents the data record in order to allow its independent interpretation. The archive is available through two directory trees which can be accessed at <a href="http://sha.stanford.edu/mwo/msm.html">http://sha.stanford.edu/mwo/msm.html</a>. The calibration of the observations is impacted by the solar surface convective flows, which produce offsets for both differential rotation and meridional circulation functions. The effects of these offsets have been reduced in this and other publications by temporal averaging.

**Keywords** Solar · Magnetogram · Dopplergram · Calibration

## 1. Introduction

This paper releases the Mt. Wilson 150-foot tower magnetic and Doppler archival data for use by the solar and space physics communities. The web resource at http://sha.stanford.edu/mwo/msm.html provides links to the released data. Earlier releases of the MWO magnetic fields are available at: Daily Average Full Disk Observations from the Third-Generation Magnetograph at MWO (DOI https://doi.org/10.25668/4w6k-9h23) and at the Harvard Dataverse. The fits format files released here are for every observation. All have been interpolated to a uniform 256 × 256 spatial grid and rotationally shifted in time to 20:00 UT using a standard differential rotation law (for the short time shifts, details do not matter). This paper provides details about the analysis of the observational data to facilitate independent analysis. These collected magnetogram and Dopplergram observations are a resource that allows the study of magnetic evolution and dynamical flows over more than four solar cycles.

A timeline summary of the history of magnetic and Doppler observations at the 150-foot Tower Telescope is given in Figure 1. Due to the start of the observations before the era of

R.K. Ulrich

Dept. of Phys. and Astro., University of Calif. at Los Angeles, 475 Portola Plaza, Los Angeles, CA 90095-1547, USA



149 Page 2 of 14 R.K. Ulrich et al.

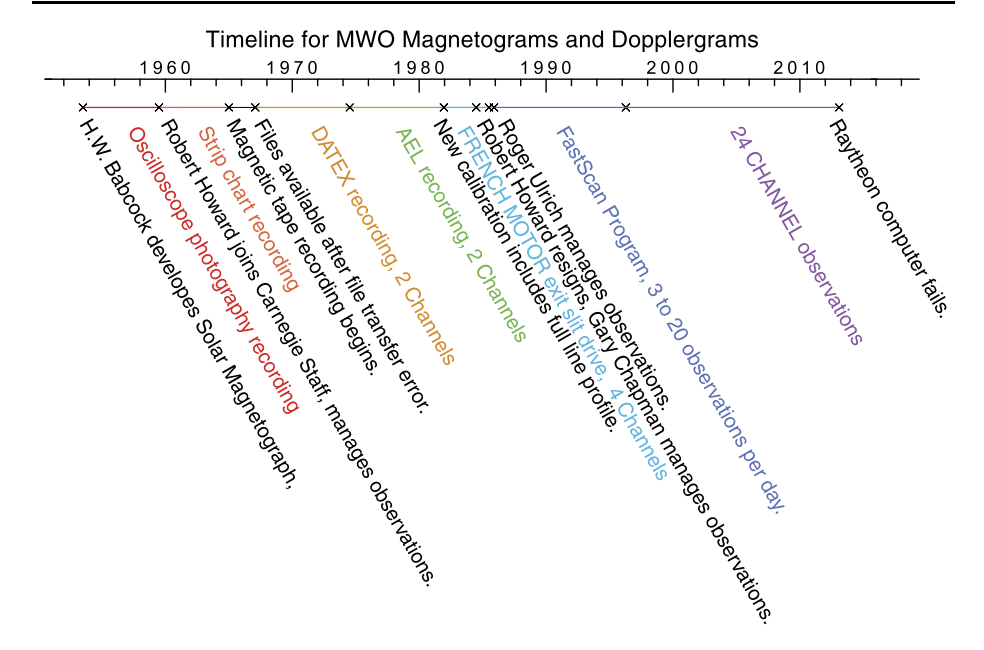


Figure 1 This timeline shows events denoted by the X symbol and intervals denoted by the horizontal line segments with varying colors. The associated texts for these intervals are in colors matching the line segments. Where the X symbols are only associated with a particular event and not a data format era, the text is black and is offset upward. There are three events at times near 1984. The associated texts are offset horizontally to enhance readability.

commonplace computers, data storage, and management began primitively and evolved over the period of the program. Events are marked on the timeline by X. Identifying text is below the timeline. Periods of different data management are indicated on the timeline by different colors of the line along with an X at the bounding times. The color of the text explaining the period matches the line color for that interval. The text associated with particular events rather than data periods is black.

The very early data used oscilloscope photographs to store the magnetogram data, and in June 1963, Howard began using an X - Y plotter with two pens of different colors. Both data sources were converted to contour synoptic maps published in the atlas by Howard, Bumba, and Smith (1969), which covers August 1959 to June 1966. A scan of this document is available from the same source as the archive data. It is our hope that data values from this resource can be extracted to a digitally available format. Then, in 1965, Howard transitioned to the use of a magnetic tape recording system to record the data in digital format. A tape handling error in 1967 lost the first two years of data, and the available data has a beginning date of 1967. The tape format changed in 1974 from binary-coded decimal to binary, allowing for greater digital resolution. The 4-channel system beginning in 1981 allowed for the regular observation of Cr II at  $\lambda 523.733$  nm. This line had been observed before but as a separate observation at a time before or after the scan of Fe I  $\lambda$ 525.022 nm. A FastScan program began in 1985 increasing the number of observations per day from 1 – 2 to 20 depending on sky conditions. Since 1996 a multi-spectral line 24-channel system has begun taking data for two additional spectral lines with five sampling pairs each (Ulrich et al. 2002) as discussed below.



Management of the observation program began with Babcock and shifted gradually to Howard, who directed the program until 1984, when he resigned from his position with the Carnegie Institute of Washington and became director of the National Solar Observatory in Tucson, AZ. Gary Chapman managed the program until 1985, when Roger Ulrich accepted the responsibility for the observations.

Section 2 describes the observing system, Section 3 goes through the current reduction steps, Section 4 gives the details about the spectral lines observed with the 24-channel system, Section 5 goes through the observing sequence, Section 6 gives the algorithms to determine the observable output, Section 7 explains how meridional circulation influences the fit to the velocities, and finally, Section 8 describes the released files.

## 2. The Observing System

The system acquired the data released here includes the following in the order traversed by the solar photons:

- Tower and coelostat mirrors.
- Mirror control system for guiding and solar image position control.
- The primary lens with focus control.
- Limb sensors on a transverse, controlled rack for image position management.
- Polarization control using K\*DP or ADP crystal to isolate the circular polarization components.
- Entrance aperture with image slicer and spectrograph entrance slit.
- The first pass through the Littrow lens.
- Dispersing grating.
- The second pass through the Littrow lens.
- Order blocking filters.
- Entrance to narrow rectangle of image reformattor or selection by a prism and blind assembly.
- A movable stage to carry detectors to follow Doppler shifts.
- Output to each photomultiplier detector produces a channel of data.
- Digitization per pixel and recording as part of the per-pixel output.

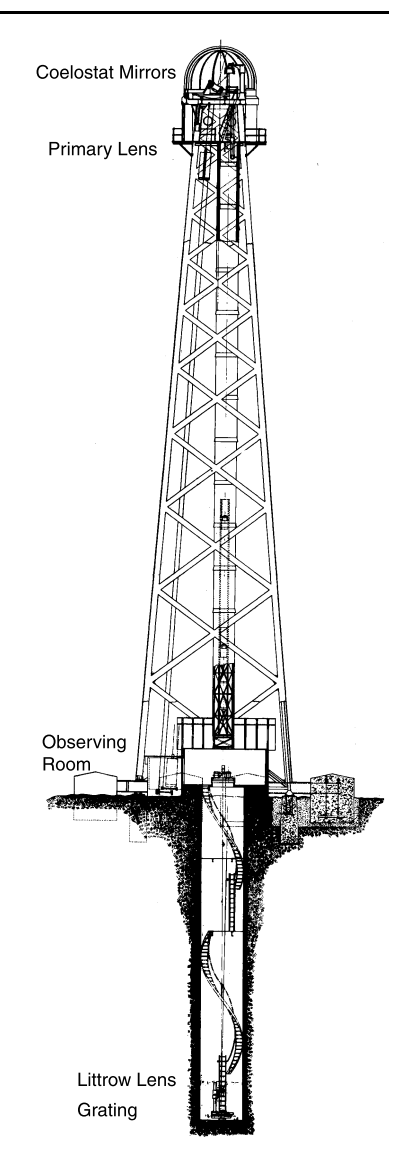
Multiple hardware and computer components coordinated these steps. Details are given at various places in this paper. These steps are shown in Figures 2 and 3.

The use of the diffraction grating spectrograph with a rapidly varying circular polarization retarder to measure magnetic fields was developed by Babcock (1953), Howard and Babcock (1960), Howard (1974, 1976), Howard, Boyden, and Labonte (1980). The work by Howard et al. (1983b) introduced the use of fiber-optic image reformattors to carry out spectral sampling. The previously used prism and blind system was subjected to inadvertent modification due to its mechanical nature. Minor shifts of the parts modified the spectral bandpass and shifted the apparent position of the incoming signal with consequent shifts in the detected Doppler velocity. The fiber-optic components can be locked firmly in place and are not subject to mechanical instabilities. Scatter in the measured solid body rotation rate coefficients dropped significantly after 1983 when the fiber-optic system was installed. These measurements continue to be influenced by the large-scale motions of the supergranulation.

The current system of photomultipliers produced counts provides 24 channels of data as described in detail by Ulrich et al. (2002). This spectrograph system takes light from an



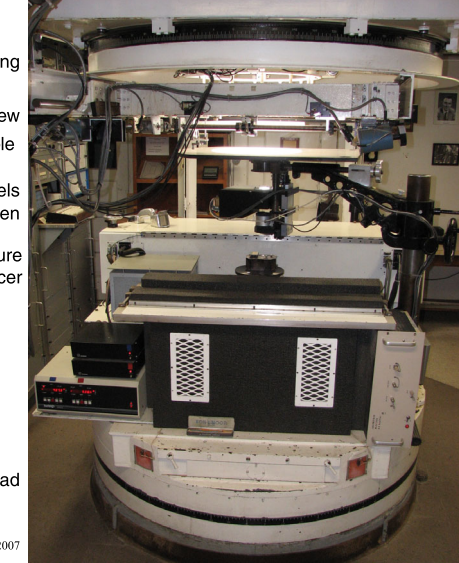
Figure 2 This is a technical drawing of the 150-foot tower telescope at MWO of what the tower was to be like after it was built. Some details are incorrect, but the main layout is correct. The coelostat mirrors guide the solar image to the optical axis and the image does not rotate unless the positions of the mirrors are changed. The daily morning and afternoon setups cause the image to have different rotational orientations, which are accommodated during setup. The objective lens, Littrow lens, and grating are in the positions shown although there is no representation of either in this drawing. The optical axis is not vertical, so dropped objects will miss the optical components. This feature proved valuable on several occasions. Image courtesy of the Observatories of the Carnegie Institution for Science Collection at the Huntington Library, San Marino, California.



entrance square through an image slicer, which produces a narrow rectangle that enters the spectrograph. The dispersed spectrum comes from the 75-foot focal length Littrow configuration. The dispersed light at the exit slit for each spectral line is captured by one of 24 reformattors each of which is a narrow rectangular fiber-optic bundle extending across the spectrum acting as an entrance slit. Each bundle is reformatted from a rectangle to a circle, surrounded by a flexible cover ending in a metal collar.

Each bundle can illuminate a photomultiplier cathode, which produces a voltage that is then converted to output pulses with a voltage-to-frequency converter. Each crest in the output wave creates a count that is added to one of two buffers per channel, which are synchronized with the oscillating variable polarizer of the Babcock system. When a buffer count is transferred to external storage, it is cleared, and a new count is begun. A separate multi-





Guider Ring Guider drive screw Light baffle table Filter wheels K\*DP Oven Entrance Aperture Image Slicer

Spectrograph Head

Photo by Larry Webster, 2007

Figure 3 A photograph of the observation room taken by Larry Webster showing components along the optical path. This photograph was taken in 2007 after most improvements had been made. The guider ring at the top rotates to accommodate the optical axis set by the coelostat mirrors. The structure is driven by the X, Y screws which respond to the limb signal from the two pairs of sensors. The control of the image can be monitored by the out-of-focus image on the light baffle table. The filter wheel allows for the insertion of blocking filters or polarizer components. The K\*DP polarizer is in a temperature-controlled box and provides variable isolation for the two circular polarization components. A table with drawing paper is inserted above the entrance aperture assembly to permit the daily sunspot drawing. The black box on the lid of the spectrograph holds the entrance aperture and the Walraven image slicer. Light enters the spectrograph through its slit after the image slicer.

channel reformattor assembly is required for each spectral line we study. Multiple bundles can be directed to a single photomultiplier, or a bundle can be capped without recording its photons. Each detecting photomultiplier provides a signal count, which we refer to as a channel, and each studied spectral sample requires a pair of channels situated on the blue and red line wings at approximately the same distance from the line core. The detailed channel configurations are shown in Figure 4 for the four spectral lines we study. Figure 4 is adapted from a similar one in Ulrich et al. (2002), with the primary difference being the addition of the numbers used to refer to each channel being recorded.

## 3. Current Reductions

The line-of-sight velocities include large contributions from rotation as well as smaller contributions from Meridional Circulation. We subtract initial constant offset contributions from these two velocity fields, so the remainder is small and largely without a latitude-dependent component. These initial offset functions were derived from early data and are largely cosmetic. This subtraction yields maps we call deviation maps, and recovery of the full rotation and circulation rates requires the restoration of these previously subtracted offsets. Our aim in our current reductions is to have all temporal variations represented in the deviation maps. The initially stored deviation maps are in binary output data files, which



149 Page 6 of 14 R.K. Ulrich et al.

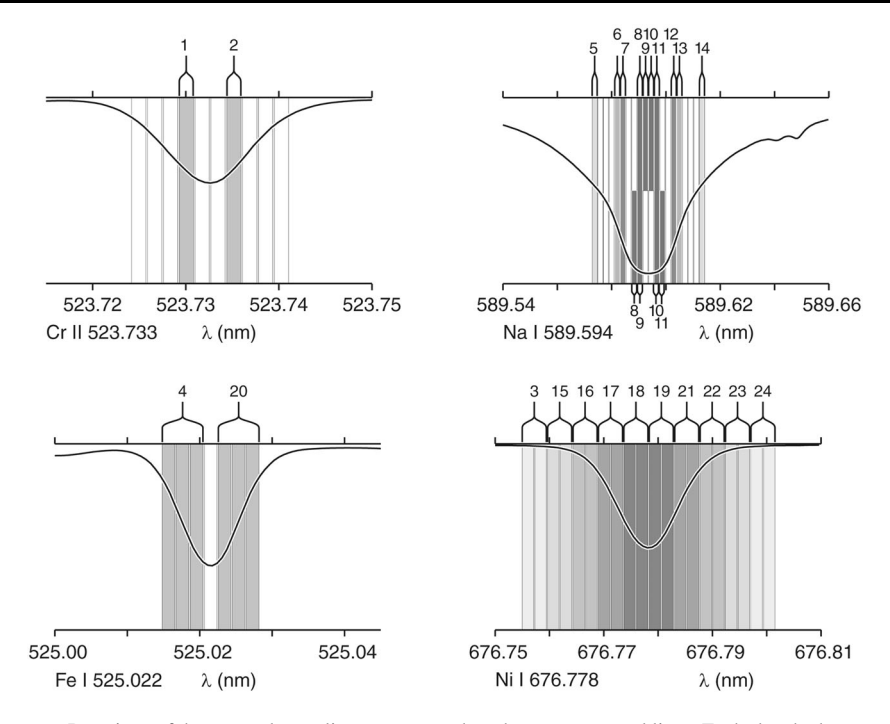


Figure 4 Drawings of the spectral samplings superposed on the target spectral lines. Each sketched rectangle represents the entrance end of a fiber-optic bundle. Each active bundle is separately configured so its output end is directed to the cathode of a photomultiplier tube. If the collar end is part of an active pair, the rectangle is grey in the figure, while if it is inactive, the rectangle is white. Active bundle pairs are shown with equal shades of grey. Channel numbers are given above each active bundle group so that, for example, the original pair of channels for  $\lambda525.022$  nm are given the numbers 4 and 20. For channels 8,11 and 9,10 the bundles were moved in August 2007 so that the sampling of the Na D1 changed. The before-change channel numbers are on top, and the after-change channel numbers are on the bottom.

we label as the 01 files. These files are a series of records which each have the location, time, and stage position s along with the four data values from the Babcock magnetogram: (x, y, t, s, A1, A2, B1, B2) where A1, A2, B1, B2 are the sums of the voltage to frequency counts and represent the intensities at the blue and red working points of a spectral line. The 1 and 2 values indicate the polarization state of the K\*DP retarder. Following Howard et al. (1983b), four quantities are calculated from these four numbers: I, Z, E and C where Z/I is essentially the Stokes V parameter, E/I is a measure of the Doppler error, and C/I is a measure of the circular polarization introduced by the telescope with its coelostat mirrors:

$$Z = \Sigma (A1 - B1 - A2 + B2),$$

$$I = \Sigma (A1 + B1 + A2 + B2),$$

$$E = \Sigma (A1 - B1 + A2 - B2),$$

$$C = \Sigma (A1 + B1 - A2 - B2).$$

The values of (x, y) are at the actual locations of each record. We also include the times for each pixel along with the positions of the spectrograph scanning stages. Due to imperfections in the scanning control system and the lack of a mechanism to place the pixels at



regular intervals of x, the grid as measured is not regular in either x or y, and the time required for the full disk scan means that the time increases continuously for the pixels.

In order to provide arrays that can be used with algorithms normally applied to image arrays, the 01 files are converted to a format we refer to as the MVI files. These files have the A1, A2, B1, B2 intensities converted into magnetic field strength: M, Doppler line-of-sight velocity: V and intensity value: I. The value of E/I is determined by the position of the spectral line relative to the scanning stage. The Doppler line-of-sight velocity depends on both this deviation and the position of the stage, which is part of the record. We have corrected the positions for differential rotation to a location appropriate for 20:00 UT. In addition we have interpolated the pixels to a finer grid in rectangular coordinates using the code mvitofits.

The output arrays from *mvitofits* are stored in three *fits* files. During the processing, corrections are applied to remove the limb shift, the solid body rotation represented by the *A* coefficient, correct for the effect of scattered light, and remove the time-dependent global velocity offset due to Earth rotation and annual orbital velocity. The initial offset values of the differential rotation as represented by the *B* and *C* coefficients are removed according to:

$$\delta V_{\text{rot}} = -R_{\odot} \sin(L) \cos(\phi) \cos(\phi_0) \left(-0.409999 \left(\sin^2(\phi) + 1.0216295 \sin^4(\phi)\right)\right),$$

where  $\delta V_{\rm rot}$  is the change in the line-of-sight component of rotation velocity in km/s due to this correction, L is the central meridian distance angle,  $\phi$  is the latitude, and  $\phi_0$  is the polar axis tilt. The B and C differential rotation coefficients were previously derived from fitting for each observation but are now left fixed. We also hold the line-of-sight component of the meridional circulation velocity as a spatially dependent function that is constant with time using the equation:

$$V_{mer} = [\cos(L) * \sin(\phi) \cos(\phi_0) - \cos(\phi) \sin(\phi_0)] [(G\sin(\phi) + H\sin(2\phi))]$$

with

$$G = -0.028692 \,\mathrm{km/s}$$
 and  $H = 0.035240 \,\mathrm{km/s}$ .

The deviations from both the differential rotation law and the meridional circulation law can then be derived from all of the observation maps.

The deviation maps are a new representation of the dynamical state of the solar surface, allowing more detailed time and latitude-dependent functions to be derived. Reductions using the polynomial fitting technique described in this section caused the appearance in the meridional circulation of a feature called "Ears". The present reduction shows that this feature is an artifact of the stiffness of the polynomial. Details are given below in Section 7.

# 4. Defining the 24-Channel Spectral Samples

After late 1995, the 24-channel system (Ulrich et al. 1991) was put into production use so that the spectral line of Na I at  $\lambda$ 589.594 nm and the Ni I line at  $\lambda$ 676.778 nm along with Fe I  $\lambda$ 525.022 nm and Cr II  $\lambda$ 523.733 nm were all measured simultaneously. The 24-channel system uses a new spectrograph grating provided by Milton-Roy, which produces the same dispersion for Fe I as the prior grating but in the 9th order instead of the 5th order. Orders are separated with narrow band filters ahead of the exit slits. As documented by Ulrich et al.



149 Page 8 of 14 R.K. Ulrich et al.

(1991), the two lines in the yellow are each sampled with a single pair of channels, while the remaining two lines are each sampled with 5 channel pairs (10 channels each). The range of altitudes in the photosphere is greatest for the sodium line. The outputs from all channels are collected simultaneously and continuously into separate buffers during the observation so that the observed differences are due to conditions at different altitudes and are not due to temporal changes.

The 24-channel system takes advantage of the flexibility afforded by the fiber-optic method of moving the exit slit photons to photomultiplier tubes. Each tube provides a signal voltage that yields the line intensity at its instantaneous working point. We take advantage of the fortuitous coincidence between three spectral regions to use the 7th, 8th, and 9th orders to simultaneously observe the spectral line used in the MDI instrument (Scherrer et al. 1995), the Na D1 line used by the GOLF instrument (Gabriel et al. 1995, 1997) and the two lines in the yellow that are used in the MWO synoptic program. The fiber-optic method was instituted by Howard et al. (1983b) with four channels sampling two spectral lines:  $\lambda 525.022$  nm and  $\lambda 523.733$  nm. The project purchased four new reformattors, with 7, 10, 20, and 20 output bundles. A new bank of 20 photomultipliers was built by the project and put into operation in 1996. The previous unit with 4 photomultipliers continued to work well and was included in the new system to provide a total of 24 channels.

With the number of photomultiplier tubes being 24 and the number of fiber-optic output bundles being 57, it is clear that not all fiber-optic outputs can be used. The problem is partly solved by using multiple bundles for some channels. In order to match the spectral sampling channels used by Howard for  $\lambda 525.022$  nm prior to our reconfigurations, we combine the output from the 7-bundle reformattor in two sets of 3 separated by an inactive bundle. With the 10-bundle reformattor we use two individual bundles separated by two inactive bundles for the sampling of the  $\lambda 523.733$  nm line. For the line  $\lambda 676.778$  nm, we use all 20 bundles in groups of 2 to sample the full spectral range of this line. Our goal was to simulate the full spectral range sampling used by the MDI instrument. A study by Evans (1999) carried out such an analysis. The channel pairs 3,24 and 15,23 do not yield useable Doppler velocities or magnetic fields and are not included in this released set of data. Finally, for the Na D1 line at  $\lambda 589.594$  nm, we used 10 bundles in 5 pairs to sample this line over a physically interesting range of altitude. The sampling bundles for  $\lambda$ 589.594 nm were changed on Aug. 15, 2007. Initially, channels 9 and 10 were at the line center with no space between them, and channels 8 and 11 measured the next pair. After that date the bundles from the innermost channels were removed and replaced by the bundles just outside the previously numbered channels 8 and 11. The channels were renumbered so that channel 8 became 9 while channel 11 became 10. The channel numbered 9 became 8 while the channel numbered 10 became 11. The separation between channels 9 and 10 remained the same as it was when the channels were numbered 8 and 11, so the 9,10 series continued the previous 8,11 series, and the measurements from 8 and 11 became a new series. The previous 9,10 series did not produce useable magnetic fields or velocities. This reconfiguration is illustrated in Figure 4 by the sequence of dark and white rectangles.

# 5. The Observing Program

After 1986, a program of fast-scans was begun wherein the entrance aperture was increased from 12 arc-sec square to 20 arc-sec square. This decreased the time for each observation from about 50 to about 20 minutes, allowing for about 3 observations per hour. Typically, 15 to 20 observations were made each day. A regular setup program precedes some of the



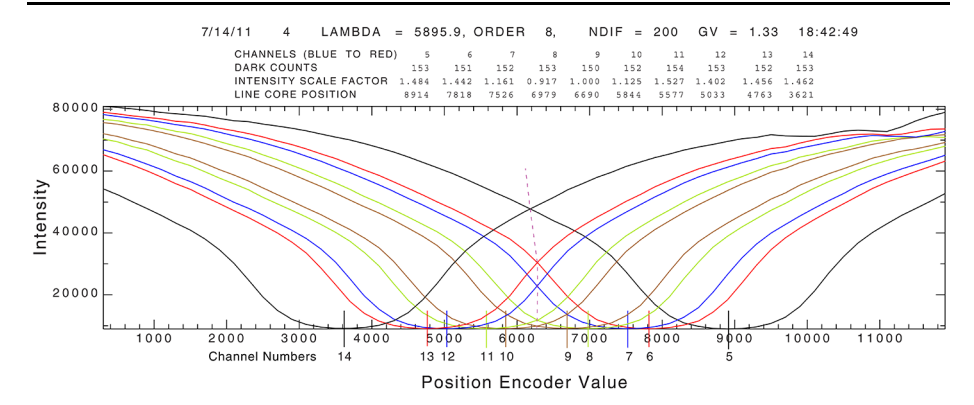


**Figure 5** This figure shows the line profiles as measured by the pickup assemblies used for the Na D1 line. The lines of information above the figure give channel numbers, the subtracted dark count, a scale factor to compensate for variations in the photomultiplier performance, and the positions of the line core in units of nm. The separations between channel pairs can be found in differences between appropriate line core positions. These separations are in encoder units and need to be multiplied by the dispersion to get the units of pm used in Table 1. The dashed magenta line goes through the points where the line intensities are equal.

observations, with typically 3 being done for each setup. The dispersion was measured during the setup by causing the servo system to balance line wing intensities on one spectral line and then another after shifting the stages to the other line. Although the shift took only about 10 seconds, that is enough for the velocity change due to the 5-minute oscillations to produce an error in the dispersion. Future reductions should replace the used dispersion with an average value derived from at least 30 measurements. The setup program also provides scans of all the lines used so that actual line profiles can be used to determine M, V and I. A typical set of line profiles derived for the Na D1 line is shown in Figure 5.

# 6. Deriving M, V and I

In a perfectly working Babcock system with a single sampling pair on a stage driven to keep the count sums for the blue and red wings equal, there would be no servo error, and the velocity would be calculated from the servo position. In practice, the servo position lags behind this position, and the intensities are never equal. In addition, only one spectral sample pair per stage can control the stage position, so all other sample pairs are held out of balance. The quantity E defined above is the difference between the polarization state average intensity on the blue wing minus the similar average on the red wing. We refer to this as the servo error E and use the ratio of E to E to calculate a correction to the servo stage position. The Zeeman effect also causes the polarized lines to be displaced oppositely for the two polarization states, giving the intensity difference quantity E. We need to convert this intensity difference into a wavelength separation.

The calculation of displacement distance and displacement wavelength requires us to know the observed line profiles as well as the spectrograph dispersion. The conversion of intensity imbalance into a Zeeman splitting displacement and a Doppler error depends on the measurement of intensity as a function of wavelength distance from the balance point of the spectrograph sampling. The initial step in setting up a magnetogram observation includes instructing the spectrograph stages to perform line scans. The stage positions are recorded with a precision screw and their digitizing controller.



149 Page 10 of 14 R.K. Ulrich et al.

Pair	Sep pm	Lim	Powers Used										
			1	2	3	4	5	6	7	8	9	10	11
MW1	52	0.20	•	•	•				•		•		
MW2	78	0.40	•	•			•						
Na D1	396	0.20	•	•			•		•		•		•
Na D1	228	0.62	•				•						
Na D1	186	0.62	•				•						
Na D1	105	0.20	•	•	•							•	
Na D1	63	0.20	•	•	•							•	
MDI	230	0.20	•	•	•	•	•	•	•	•	•	•	
MDI	142	0.30	•	•	•		•		•	•		•	
MDI	58	0.15	•	•	•								

Table 1 Polynomial Properties.

The measured line profile allows us to convert the intensity differences into a displacement from the working point. Each pair consists of a blue profile and a red profile. Only the blue wing of the blue profile is needed, while only the red wing of the red profile is needed, so we join the utilized wings at the line core and treat the result as a single profile. Line profiles are commonly described as intensity as a function of distance from the line center. We reverse this and represent the displacement as a function of E/I with a polynomial that has a form that uniquely represents each sampling pair:

$$\Delta = \sum_{n=1}^{n_{max}} \left[ a_n (E/I)^n + b_n [1 - \cos(\rho)] (E/I)^n \right],$$

where  $\Delta$  is the micron Doppler unit offset, which we need to know, and  $n_{max}$  ranges up to 11. The second part of this equation allows us consider that the line profiles depend on center-to-limb distance  $\rho$ . To get the wavelength shift  $\Delta$  needs to be multiplied by the dispersion. The values of  $a_n$  and  $b_n$  are in micron Doppler units. The set of n values is different for each working pair. Due to the varying line profiles, especially at the different working points, each working pair is treated differently. The values of all the  $a_n$  and  $b_n$  are determined from each setup scan, so many of these coefficients exist. If the value of |E/I| exceeds a limit given in Table 1, column 3 titled Lim, the point is not evaluated and is left out of any plot or calculation. Values for  $a_1$  are shown in Figure 6.

For brevity, we designate the four studied lines with abbreviations MW1:  $\lambda523.733$  nm, MW2:  $\lambda525.022$  nm, Na D1:  $\lambda589.594$  nm and MDI:  $\lambda676.778$  nm. The ten pairs are listed in Table 1. The top line lists the polynomial powers, which can be used in the fit, and the table indicates the powers used by a  $\bullet$  symbol in the appropriate column, while if the power was not used, there is the period in the column. The line fitting was tailored to each channel pair except for the Na D1 case with a separation of 105 pm for which the configuration from the pair with a separation of 63 pm was used.

After the fitting coefficients are available, the displacements can be found from  $\Delta$  for each observed sample pair. The velocity requires the addition of the stage position known and recorded for each observed pixel, while the separation between the polarization states yields the magnetic field. The results of applying the fitting coefficients are stored in the MVI files, which are then converted to the *fits* files that are included as the primary output.



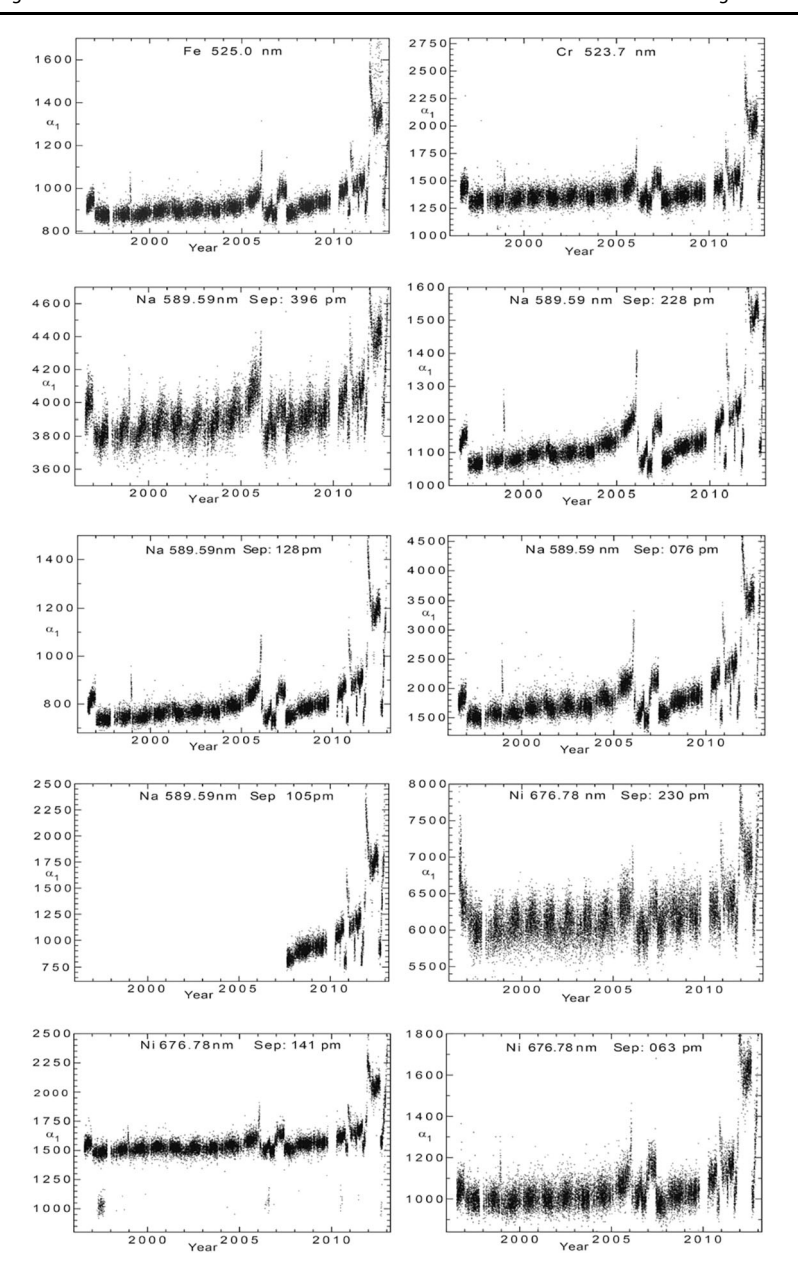


**Figure 6** Plots of the time dependence of the  $a_1$  fitting coefficients. Each spectral sampling has its own fitting coefficient. The remaining  $a_n$  could also be shown, but their variability is similar to that of  $a_1$ . The values of all fitting coefficients are available for use if needed. The fitting coefficients represent the actual line profiles at the time of the observation. Some noise impacts these profiles due to supergranulation. Changes in the line profile coefficients occur due to instrument changes and due to photomultiplier aging or replacement.

As an indication of the stability of the system, we include Figure 6, which shows plots of



149 Page 12 of 14 R.K. Ulrich et al.

the  $a_1$  coefficients for each of the pairs. Note that there is no  $a_0$  or  $b_0$  because the intensities of the working points match after the line position is shifted according to E/I.

#### 7. Identification of Meridional Circulation

A topic of the publication Howard, Boyden, and Labonte (1980) was the feature named "Ears", which is a change in the systematic line-of-sight velocity toward the East and West limbs. The authors were unable to identify a cause for these shifts and concluded they were instrumental in origin. Fortunately there is a simple explanation – the shifts are due to Meridional Circulation caused by solar rotation. In the radiative interiors of stars, this phenomenon is known as Eddington-Sweet circulation, named after the first authors Eddington (1929), Sweet (1950). The process was discussed extensively by Mestel (1953), Mestel and Moss (1986), and others to consider the question as to whether or not it could keep nuclear evolution from producing a gradient in helium abundance by mixing the star. A concise physical discussion is given by Schwarzschild (1958) in §21. The general conclusion is that the Eddington-Sweet velocities are too small to influence the nuclear abundance gradient and are too small to be significant for surface flows. In addition, the E-S circulation induced by rotation alone produces a flow from the pole toward the equator.

In contrast to the solar core, for the surface convection zone Gilman (1972, 1976) and Gilman (1977) showed that rotation and convection can combine to produce a significant equator to pole flow. Based on these models, Duvall (1979) carried out tests at the Stanford Solar Observatory (now known as the Wilcox Solar Observatory WSO) which showed that convection modified by rotation could generate a meridional flow. We have dealt with this flow by deriving the limb shift from an equatorial band 4 bins wide (out of 34 for the full solar diameter) and using that shift along all position angles around the solar image. An extensive discussion of this approach was given by Ulrich et al. (1988) and extended by Ulrich (2010). The effect of the meridional circulation shows up as deviations from constant lineof-sight velocity for regions away from the equator. Our series' representation of rotation over the solar surface does not include the three terms having coefficients labeled D, E, and F by Howard et al. (1983a). However, the sum of those terms as published by Howard et al. (1983a) provides a reasonable estimate for the meridional circulation. Our treatment of the Meridional Circulation is now described in Section 3. Reductions with these methods have yielded interesting time-dependent features of the surface velocities (Ulrich, Tran, and Boyden 2022, 2023).

## 8. The Released Files

The released files are grouped by year and month from 1967 to 2012. The years before 1996 have one or two wavelength samples, while those after 1996 have 9 or 10 wavelength samples, as discussed above. Also, those before 1996 do not have the intensity *fits* files. After 1985, the number of observations per day increased from 1-2 to 1-20. For each year, there is a file not included in the release, but, on request, it can be provided with the name mgprnt, which is an ASCII version of the reduction printout. This file includes a large number of quantities, many of which represent obscure variables. Some of the tables in the mgprnt files may be of interest. The size of the mgprnt files is significant (0.5 to 0.9 Tbytes/year), and extraction of the variables requires some effort. The released files include diagnostic pdf files that plot the variables. These can be useful in determining the quality of the observations.



The file names include useful identification characteristics:

DP00\_5895104\_00\_1070816\_1798

where the first letter is D, I, or M indicate Doppler velocity, Intensity, or Magnetic field, respectively. The P00 is a sequence number, 5895104 is the spectrum sample, in this case, for the Na D1 line with a separation of 104 pm [note that the separations are measured from the scans and show small variations; in this case, the earlier measurement gave 105 pm, as shown in Figure 6]. In the years before 1982 after the wavelength designation, the letters MWO are used instead of the wavelength separation. This notation transition is irregular relative to the date of observation. The 00\_1 is another sequence number, and 070816\_1798 is the date and time in the format yymmdd\_tttt with tttt being the fractional hour. The leading two digits of the year number are left off and understood to be 19 if the year is greater than 30 and 20 otherwise. The hour is in UT.

The diagnostic .pdf files have slightly different names:

P5250 07820070829 2244

where the P indicates the .pdf nature of the file and the spectral sampling 5250\_078 and yyyymmdd\_tttt comes next. A naming transition before 1982 like that for the data files also applies to the diagnostic files.

A link to the files is: http://sha.stanford.edu/mwo/msm.html

Acknowledgements The Mt. Wilson Observatory project was started by the Carnegie Institution of Washington and financed by that institution until 1984 when management and funding were transferred to UCLA. Before the transfer funding was provided by the US Navy through its Office of Naval Research as well as NASA and NSF. After the transfer NASA and NSF provided most of the support along with continuing support from ONR. Current support comes from NSF through grant 2000994 while earlier support came from the NSF through grant AGS-0958779 and NASA through grants NNX09AB12G and HMI subcontract 16165880. Over the years additional funding has come from these two agencies as well as the ONR and NOAA. Ulrich and Boyden are supported by retirement funds while Tran is supported by the NSF grant. The observatory is managed by the Mt. Wilson Institute. Todd Hoeksema provided helpful comments on drafts of this paper which resulted in its improvement. Rick Bogart set up the JSOC storage of these data at the site sha.stanford. edu/mwo/msm.html and managed the loading of the data into this site.

**Author contributions** RKU carried out the analysis, prepared some figures, drafted the submission. JEB developed the code, did the initial reductions and analysis. TT drafted parts of the submission and prepared the 2 dimensional plots. All authors reviewed the manuscript.

**Data Availability** The data discussed in this paper is being released in digital form and can be used by others for additional analysis and research.

#### **Declarations**

**Competing interests** The authors declare no competing interests.

Open Access This article is licensed under a Creative Commons Attribution 4.0 International License, which permits use, sharing, adaptation, distribution and reproduction in any medium or format, as long as you give appropriate credit to the original author(s) and the source, provide a link to the Creative Commons licence, and indicate if changes were made. The images or other third party material in this article are included in the article's Creative Commons licence, unless indicated otherwise in a credit line to the material. If material is not included in the article's Creative Commons licence and your intended use is not permitted by statutory regulation or exceeds the permitted use, you will need to obtain permission directly from the copyright holder. To view a copy of this licence, visit http://creativecommons.org/licenses/by/4.0/.

## References

Babcock, H.W.: 1953, The solar magnetograph. Astrophys. J. 118, 387. DOI. ADS.



149 Page 14 of 14 R.K. Ulrich et al.

- Duvall, T.L. Jr.: 1979, Large-scale solar velocity fields. Solar Phys. 63, 3. DOI. ADS.
- Eddington, A.S.: 1929, Internal circulation in rotating stars. Mon. Not. Roy. Astron. Soc. 90, 54. DOI. ADS.
- Evans, S.E.: 1999, MDI and GOLF simulation and intercomparison via the Mt. Wilson 150-foot tower. Ph. D. Thesis. ADS.
- Gabriel, A.H., Grec, G., Charra, J., Robillot, J.-M., Roca Cortés, T., Turck-Chièze, S., Bocchia, R., Boumier, P., Cantin, M., Cespédes, E., Cougrand, B., Crétolle, J., Damé, L., Decaudin, M., Delache, P., Denis, N., Duc, R., Dzitko, H., Fossat, E., Fourmond, J.-J., García, R.A., Gough, D., Grivel, C., Herreros, J.M., Lagardère, H., Moalic, J.-P., Pallé, P.L., Pétrou, N., Sanchez, M., Ulrich, R., van der Raay, H.B.: 1995, Global Oscillations at Low Frequency from the SOHO mission (GOLF). Solar Phys. 162, 61. DOI. ADS.
- Gabriel, A.H., Charra, J., Grec, G., Robillot, J.-M., Roca Cortés, T., Turck-Chièze, S., Ulrich, R., Basu, S., Baudin, F., Bertello, L., Boumier, P., Charra, M., Christensen-Dalsgaard, J., Decaudin, M., Dzitko, H., Foglizzo, T., Fossat, E., García, R.A., Herreros, J.M., Lazrek, M., Pallé, P.L., Pétrou, N., Renaud, C., Régulo, C.: 1997, Performance and early results from the GOLF instrument flown on the SOHO mission. Solar Phys. 175, 207. DOI. ADS.
- Gilman, P.A.: 1972, Nonlinear Boussinesq convective model for large scale solar circulations. Solar Phys. 27, 3. DOI. ADS.
- Gilman, P.A.: 1976, Theory of convection in a deep rotating spherical shell, and its application to the Sun. In: Bumba, V., Kleczek, J. (eds.) *Basic Mechanisms of Solar Activity* 71, 207. ADS.
- Gilman, P.A.: 1977, Nonlinear dynamics of Boussinesq convection in a deep rotating spherical shell. I. Geophys. Astrophys. Fluid Dyn. 8, 93. DOI. ADS.
- Howard, R.: 1974, Studies of solar magnetic fields. I The average field strengths. Solar Phys. 38, 283. ADS.
   Howard, R.: 1976, The Mount Wilson solar magnetograph scanning and data system. Solar Phys. 48, 411.
   DOI. ADS.
- Howard, R., Babcock, H.W.: 1960, Magnetic fields associated with the solar flare of July 16, 1959. *Astrophys. J.* **132**, 218. DOI. ADS.
- Howard, R., Boyden, J.E., Labonte, B.J.: 1980, Solar rotation measurements at Mount-Wilson part one analysis and instrumental effects. *Solar Phys.* 66, 167. DOI. ADS.
- Howard, R., Bumba, V., Smith, S.F.: 1969, Atlas of solar magnetic fields. ADS.
- Howard, R., Adkins, J.M., Boyden, J.E., Cragg, T.A., Gregory, T.S., Labonte, B.J., Padilla, S.P., Webster, L.: 1983a, Solar rotation results at Mount-Wilson part four results. *Solar Phys.* 83, 321. DOI. ADS.
- Howard, R., Boyden, J.E., Bruning, D.H., Clark, M.K., Crist, H.W., Labonte, B.J.: 1983b, The Mount Wilson magnetograph (Report from a solar institute). *Solar Phys.* 87, 195. ADS.
- Mestel, L.: 1953, Rotation and stellar evolution. Mon. Not. Roy. Astron. Soc. 113, 716. DOI. ADS.
- Mestel, L., Moss, D.L.: 1986, On mixing the Eddington-sweet circulation. Mon. Not. Roy. Astron. Soc. 221, 25. DOI. ADS.
- Scherrer, P.H., Bogart, R.S., Bush, R.I., Hoeksema, J.T., Kosovichev, A.G., Schou, J., Rosenberg, W., Springer, L., Tarbell, T.D., Title, A., Wolfson, C.J., Zayer, I. MDI Engineering Team: 1995, The Solar Oscillations Investigation Michelson Doppler Imager. Solar Phys. 162, 129. ADS.
- Schwarzschild, M.: 1958, Structure and evolution of the stars. ADS.
- Sweet, P.A.: 1950, The importance of rotation in stellar evolution. Mon. Not. Roy. Astron. Soc. 110, 548. DOI.
  ADS
- Ulrich, R.K.: 2010, Solar meridional circulation from Doppler shifts of the Fe I line at 5250 Å as measured by the 150-foot solar tower telescope at the Mt. Wilson observatory. *Astrophys. J.* **725**, 658. DOI. ADS.
- Ulrich, R.K., Tran, T., Boyden, J.E.: 2022, Polar upwelling at three sunspot minima. *Res. Note Am. Astron. Soc.* 6, 181. DOI. ADS.
- Ulrich, R.K., Tran, T., Boyden, J.E.: 2023, Photospheric velocities measured at Mt. Wilson show rotational and poleward velocity deviations compose the torsional oscillations. Solar Phys. 298, 123. DOI. ADS.
- Ulrich, R.K., Boyden, J.E., Webster, L., Padilla, S.P., Snodgrass, H.B.: 1988, Solar rotation measurements at Mount Wilson. V Reanalysis of 21 years of data. *Solar Phys.* 117, 291. ADS.
- Ulrich, R.K., Webster, L., Boyden, J.E., Magnone, N., Bogart, R.S.: 1991, A system for line profile studies at the 150-foot tower on Mount Wilson. *Solar Phys.* **135**, 211. ADS.
- Ulrich, R.K., Evans, S., Boyden, J.E., Webster, L.: 2002, Mount Wilson synoptic magnetic fields: improved instrumentation, calibration, and analysis applied to the 2000 July 14 flare and to the evolution of the dipole field. Astrophys. J. Suppl. 139, 259. ADS.

**Publisher's Note** Springer Nature remains neutral with regard to jurisdictional claims in published maps and institutional affiliations.

